A comprehensive study on the electrochemical advanced oxidation of antihypertensive captopril in different cells and aqueous matrices

Alexsandro J. dos Santos, Pere L. Cabot, Enric Brillas**, Ignasi Sirés*

Laboratori d'Electroquímica dels Materials i del Medi Ambient, Departament de Química Física, Facultat de Química, Universitat de Barcelona, Martí i Franquès 1-11, 08028 Barcelona, Spain

* Corresponding author: *E-mail address*: i.sires@ub.edu (I. Sirés)

** Corresponding author: *E-mail address*: brillas@ub.edu (E. Brillas)

Abstract

Anodic oxidation with electrogenerated H_2O_2 (AO-H_2O_2) of 130 mL of antihypertensive drug captopril was studied in sulfate medium, urban wastewater and synthetic urine using a BDD, Pt or IrO_2 anode and an air-diffusion cathode. Oxidants were $^{\bullet}OH$ formed during O_2 evolution and active chlorine formed via anodic oxidation of Cl^-. Drug removal decreased as: BDD > Pt > IrO_2. The effect of pH and current density was examined. Further, 2.5 L of drug solutions in the same matrices with Fe^{2+} at pH 3.0 were treated by solar photoelectro-Fenton (SPEF) using a solar pre-pilot flow plant with a Pt/air-diffusion cell and a planar photoreactor. In sulfate medium, SPEF outperformed AO-H_2O_2 and electro-Fenton because of the efficient Fe^{3+} photoreduction. Low mineralization was achieved by the small generation of photoactive Fe(III)-carboxylate complexes. In urban wastewater, captopril was more rapidly removed due to active chlorine Two heterocyclic derivatives and four aliphatic acids were detected.

Keywords: Anodic oxidation; Pharmaceutical; Solar photoelectro-Fenton; Urban wastewater; Urine

1. Introduction

Recently, the great effectiveness of the solar photoelectro-Fenton (SPEF) process for the removal of recalcitrant and persistent organic pollutants from synthetic and real wastewater has been shown [1-3]. SPEF is an environmental-friendly electrochemical advanced oxidation process (EAOP) that destroys the organic molecules by the simultaneous action of hydroxyl radical ($^{\bullet}OH$) generated on site and UVA photons directed toward the solution. The $^{\bullet}OH$ possesses a great ability to non-selectively attack the organic structures due to its high standard redox potential (E^{o}) of 2.8 V|SHE [4,5].

In SPEF process, the photolytic action of sunlight enhances the performance of a simpler but more widespread EAOP like electro-Fenton (EF) [6-8]. In EF, the weak oxidant H_2O_2 (E^{o} = 1.76 V|SHE) is generated from O_2 reduction at the cathode of an electrolytic cell via reaction (1). This reaction becomes very efficient using carbonaceous electrodes, including carbon-polytetrafluoroethylene (PTFE) [9-11] and carbon felt [12-14]. In a typical undivided cell, H_2O_2 is partly oxidized to O_2 at the anode M, originating the weaker physisorbed hydroperoxyl radical ($M(HO_2^{\bullet})$, E^{o} = 1.44 V|SHE) as intermediate from reaction (2) [5,15].

$$O_2 + 2H^+ + 2e^- \rightarrow H_2O_2 \quad (1)$$

$$M + H_2O_2 \rightarrow M(HO_2^{\bullet}) + H^+ + e^- \quad (2)$$

EF was developed from anodic oxidation process with cathodic H_2O_2 electrogeneration (AO-H_2O_2), which involves the destruction of organics either by H_2O_2 or, to a much larger extent, by physisorbed $M(^{\bullet}OH)$ formed from water discharge according to reaction (3) [16-18]:

$$M + H_2O \rightarrow M(^{\bullet}OH) + H^+ + e^- \quad (3)$$

The nature of the anode M is the most influential factor controlling reaction (3). Non-active boron-doped diamond (BDD) electrodes are known to possess a higher oxidation power than active Pt and dimensionally stable anodes like IrO_2 [19,20]. This general trend can be modulated

upon production of other oxidizing agents in selected media in which the action of M(•OH) is affected. For example, in chloride medium, the oxidant active chlorine can be additionally formed, which can be either beneficial or detrimental [16,21].

In systems equipped with the aforementioned types of cathodes and anodes, the presence of Fe^{2+} as catalyst in the acidic solution promotes the occurrence of Fenton's reaction (4) [7,21,22]. The catalyst can be continuously regenerated from cathodic Fe^{3+} reduction, but the oxidation power is substantially enhanced under SPEF conditions. The exposure of the treated solution to sunlight radiation allows that the incident UVA photons photoreduce the main generated Fe^{3+} species via reaction (5) and photodecompose the Fe(III)-carboxylate complexes according to the general reaction (6) [1,11,23,24].

$$Fe^{2+} + H_2O_2 \rightarrow Fe^{3+} + {}^{\bullet}OH + OH^- \quad (4)$$

$$Fe(OH)^{2+} + h\nu \rightarrow Fe^{2+} + {}^{\bullet}OH \quad (5)$$

$$Fe(OOCR)^{2+} + h\nu \rightarrow Fe^{2+} + CO_2 + R^{\bullet} \quad (6)$$

Several works have shown the viability of the SPEF treatment to remove aromatic and heteroaromatic drugs from acidic wastewater [7,25-28]. One of the main conclusions is that, unlike AO-H_2O_2, similar results can be obtained using active and non-active anodes because of the concomitant action of UV photons on reaction intermediates [7,21,29]. However, less is known about the destruction of heterocyclic drugs, which are expected to be more recalcitrant.

Captopril ((2*S*)-1-[(2*S*)-2-methyl-3-sulfanylpropanoyl]pyrrolidine-2-carboxylic acid, $C_9H_{15}NO_3S$) is a widely used heterocyclic thiolated antihypertensive drug. It acts as an inhibitor of the angiotensin-converting enzyme to regulate blood pressure, also being used in the management of diabetic nephropathy and heart failure after myocardial infarction [30]. However, about 40-50% of administered captopril is excreted unmetabolized via urine, whereas the rest is converted to disulfide and other metabolites [31]. This results in a large presence of

this drug in influents of municipal wastewater treatment facilities, attaining high contents up to 2.3 μg L^{-1} [32,33]. In surface water, it can induce toxicity in crustaceans like daphnids and the common carp *Cyprinus carpio* [34]. Several works have described the chemical oxidation of captopril by bromate and bromine [35], quinolinium dichromate [36] and laccase [37]. As far as we know, only Freitas et al. [30] have assessed its removal by AOPs, addressing the study of heterogeneous photocatalysis with TiO_2/UVC. Total degradation of captopril was achieved after 120 min, although the mineralization was only 9.1%, suggesting the generation of highly recalcitrant by-products. In contrast, direct UVC photolysis under analogous conditions yielded 93% degradation with 2.9% mineralization. The use of powerful EAOPs could then become an alternative to achieve a faster degradation and mineralization.

This work aims to clarify the electrochemical destruction of captopril in different aqueous matrices. First, the experiments were performed under AO-H_2O_2 conditions using a small volume of 130 mL, in order to test the oxidation ability of BDD, Pt and IrO_2 anodes in synthetic sulfate medium as a model matrix. The process was further evaluated in urban wastewater and synthetic urine, examining the effect of pH and current density (*j*) on the oxidation power. Afterwards, the SPEF process was investigated in the three aqueous matrices using a 2.5 L solar pre-pilot flow plant equipped with a Pt/air-diffusion cell coupled with a planar photoreactor. The effect of *j* and drug content on the SPEF performance was studied, and comparative AO-H_2O_2 and EF assays were made to confirm the superiority of SPEF process. Finally, the main reaction by-products were identified by gas chromatography-mass spectrometry (GC-MS).

2. Materials and methods

2.1. Chemicals

Captopril (CAS number 62571-86-2, M = 217.29 g mol^{-1}, 98% purity) was purchased from Sigma-Aldrich and used as received. Analytical grade sulfuric acid (98% purity) and sodium hydroxide pellets needed for pH adjustment were from Acros and Panreac, respectively.

Analytical grade sodium sulfate and iron(II) sulfate heptahydrate were acquired from Prolabo. The analytical solutions were prepared using a Merck Millipore Milli-Q ultrapure water system (resistivity >18.2 MΩ cm). The reagents for the preparation of the synthetic urine and the analytical solutions were of analytical or HPLC grade purchased from Merck and Panreac.

2.2. Aqueous matrices

The aqueous matrices used to dissolve captopril were:

(i) A 0.050 M Na_2SO_4 solution, prepared with Milli-Q or deionized water to perform the trials at 130-mL and 2.5-L scale, respectively;

(ii) Urban wastewater collected from the secondary clarifier of a municipal facility. The water was preserved at 4 ºC once obtained and its main characteristics were: pH = 7.2, conductivity = 1.3 mS cm^{-1}, total organic carbon (TOC) = 12.0 mg C L^{-1}; cations contained (mg L^{-1}): Fe^{2+} (0.11), NH_4^+ (37.5), Mg^{2+} (41.1), K^+ (47.4), Ca^{2+} (130) and Na^+ (213); anions (mg L^{-1}): NO_2^- (2.03), NO_3^- (5.21), SO_4^{2-} (131) and Cl^- (415);

(iii) Synthetic urine prepared with Milli-Q water for the AO-H_2O_2 treatment at 130-mL scale, with the following composition (in mM) [38]: urea (NH_2CONH_2, 55.6), uric acid ($C_5H_4N_4O_3$, 0.29), creatinine ($C_4H_7N_3O$, 1.47), KCl (13.4), $MgSO_4$ (1.41), $(Ca)_3(PO_4)_2$ (0.10), $(NH_4)_2HPO_4$ (0.63) and Na_2CO_3 (1.57);

(iv) Three synthetic urine solutions prepared with deionized water for SPEF trials:

- Urine 1: 13.9 mM urea + 0.07 mM uric acid + 0.37 mM creatinine;
- Urine 2: 27.8 mM urea + 0.15 mM uric acid + 0.73 mM creatinine; and
- Urine 3: 55.6 mM urea + 0.29 mM uric acid + 1.47 mM creatinine.

2.3. Electrolytic assays

The AO-H_2O_2 trials were carried out at 130-mL scale using an undivided two-electrode cell. The solution was stirred with a magnetic follower at 600 rpm and its temperature was kept

at 35 ºC by recirculating thermostated water through a jacket surrounding the cell. The anode was a BDD thin film deposited onto Si, purchased from NeoCoat, Pt (99.999% purity) purchased from SEMPSA or IrO_2-coated Ti plate purchased from NMT Electrodes. The cathode was a carbon-PTFE air-diffusion electrode purchased from Sainergy Fuel Cell, which was fitted in a cylindrical polypropylene support and fed with air at 1 L h^{-1} for H_2O_2 production from reaction (1). The interelectrode gap was always 1 cm and each electrode area was 3 cm^2. Galvanostatic assays were made with an Amel 2049 potentiostat-galvanostat, connected to a Demestres 601BR digital multimeter for continuous cell voltage monitoring. Cleaning/activation of electrodes was carried out as described elsewhere [29].

The SPEF experiments were performed in a solar pre-pilot flow plant constructed in our laboratory [11,39]. A filter-press one-compartment electrochemical reactor containing two electrodes in parallel, separated 1.2 cm, was employed. The anode was a 20 cm^2 Pt plate (99.999% purity) from SEMPSA and the cathode was a 20 cm^2 carbon-PTFE air-diffusion electrode from Sainergy Fuel Cell. The back side of this cathode was exposed to a gas chamber in which air was pumped at 4.5 L h^{-1} for H_2O_2 production. A solar planar photoreactor was connected to the outlet of the electrolytic cell. It consisted in a polycarbonate box of 24.0 cm × 24.0 cm × 2.5 cm (i.e., 600 mL irradiated volume), tilted 41º (latitude of our balcony in Barcelona) and with a mirror at the bottom to enhance the photon usage. The solution of 2.5 L placed in the reservoir was recirculated through the plant using a centrifugal pump, consecutively flowing toward the flowmeter, two heat exchangers, the electrolytic cell and the photoreactor before being received back into the reservoir. A liquid flow rate of 180 L h^{-1} and a temperature of 35 ºC were kept constant in all the assays. These were carried out under galvanostatic conditions and the constant *j* was provided by a Grelco GVD310 power supply, which displayed the instantaneous cell voltage. Comparative AO-H_2O_2 and EF trials were made by covering the elements with an opaque cloth. The SPEF runs were performed in sunny and

clear days of August-September of 2019. The incident average UV irradiance was of 32.3 W m^{-2}, as measured with a Kipp & Zonen CUV 5 radiometer.

2.4. Apparatus and analytical procedures

The solution pH, conductivity and concentrations of cations, anions and chlorine active were measured as reported in earlier work [29]. The H_2O_2 content was determined by the standard Ti(IV) colorimetric method using a Shimadzu 1800 UV/Vis spectrophotometer set at λ = 408 nm [40]. All the samples withdrawn from treated solutions were immediately conditioned by using PTFE filters (0.45 μm) from Whatman.

The decay of captopril concentration was monitored by reverse-phase HPLC using a Waters system that included a photodiode array detector (PDA). The liquid chromatograph was equipped with a BDS Hypersil C18 5μm, 250 mm × 4.6 mm, column at 25 ºC and the detection was made at λ = 290 nm. The mobile phase was a 60:40 (v/v) acetonitrile/water (10 mM KH_2PO_4, pH 3) mixture eluted at 1.0 mL min^{-1}. The chromatograms displayed a defined peak for captopril at retention time (t_r) of 3.6 min.

The mineralization of drug solutions was followed by the decay of their solution TOC, evaluated with a Shimadzu VCSN TOC analyzer using the non-purgeable organic carbon (NPOC) method (reproducibility of ±1%). Duplicate assays were made for captopril and TOC analyses, and average values with their error bars (95% confidence interval) are depicted.

The specific energy consumption per unit TOC mass (EC_{TOC}) in each run at electrolysis time t (in h) was obtained according to Eq. (7) [15]:

$$EC_{TOC}\ (\text{kWh (g TOC)}^{-1}) = \frac{E_{cell}\, I\, t}{V \triangle(\text{TOC})_{exp}} \qquad (7)$$

where E_{cell} is the average cell voltage (in V), I is the applied current (in A), V is the solution volume (in L) and $\triangle(\text{TOC})_{exp}$ is the TOC abatement (in mg C L^{-1}).

The main by-products formed from captopril degradation upon SPEF treatment of a 0.230 mM drug solution with 0.050 M Na_2SO_4 at j = 50 mA cm^{-2} were identified by GC-MS with the same equipment and procedure described in earlier work [28]. The analysis was made with an Agilent Technologies system containing either a polar HP INNOWax or a non-polar Teknokroma Sapiens-X5ms column, both of 0.25 μm, 30 m × 0.25 mm. The compounds were identified by comparison with the NIST05 MS database.

3. Results and discussion

3.1. AO-H_2O_2 treatment of captopril solutions at small scale

3.1.1. Captopril removal using different anodes in acidic aqueous matrices

The first AO-H_2O_2 trials were carried out at small scale, treating 130 mL of 0.230 mM captopril solutions prepared either in pure sulfate medium, urban wastewater or synthetic urine at pH 3.0 using a BDD, Pt or IrO_2 anode at j = 33.3 mA cm^{-2}. The solution pH did not change during these electrolyses. Fig. 1a-c show the corresponding normalized decays of drug concentration. Table 1 summarizes the maximum degradation percentage achieved at a given electrolysis time. Based on all these results, it can be concluded that the degradation was always enhanced in the order: IrO_2 < Pt < BDD, regardless of the matrix. Moreover, captopril was much more slowly removed in the Na_2SO_4 solution (see Fig. 1a). Considering for example the most powerful anode (i.e., BDD), total drug disappearance was attained after 120 min in this medium, whereas a much shorter time of about 60 min was needed in urban wastewater and synthetic urine (see Table 1). The same trends can be seen using the Pt and IrO_2 anodes in Fig. 1a-c. The use of BDD in sulfate medium allows the preeminent drug oxidation upon the attack of BDD(•OH) formed from reaction (3). The slower decay with Pt and IrO_2 can be explained by the lower oxidation power of Pt(•OH) and IrO_2(•OH), respectively [5,16]. The quicker degradation in the other two matrices can then be ascribed to the simultaneous action of

chlorine, produced via anodic oxidation of Cl^- ion (see content in subsection 2.2) according to reaction (8). Subsequent hydrolysis yields HClO via reaction (9), and this oxidant becomes the predominant active chlorine species at pH 3.0, with E^o = 1.49 V|SHE [3,41].

$$2Cl^- \rightarrow Cl_2 + 2e^- \quad (8)$$

$$Cl_2 + H_2O \rightarrow HClO + Cl^- + H^+ \quad (9)$$

Fig. 1d-f present the pseudo-first-order kinetic analysis of captopril concentration decays discussed above. These profiles suggest that all the AO-H_2O_2 treatments are limited by the mass transport of Cl^- ion and reactants toward the anode, where a small and steady concentration of oxidizing species (HClO and/or BDD($^\bullet$OH), Pt($^\bullet$OH), IrO_2($^\bullet$OH)) is produced. Table 1 summarizes the resulting pseudo-first-order rate constants for captopril removal (k_1), with good *R*-squared > 0.980. In sulfate medium, the higher oxidation power of BDD($^\bullet$OH) was confirmed by a k_1-value that was 3.2-fold and 4.2-fold greater than that determined with Pt and IrO_2, respectively. In wastewater and synthetic urine, the k_1-value with BDD was increased more than threefold, suggesting the larger destruction of the drug by HClO.

Table 1 also highlights the decreasing TOC removal percentage as BDD was successively replaced by Pt and IrO_2, going down from 17% to 9.4% and 6.2%, respectively, at 120 min in sulfate medium (initial TOC = 25 mg C L^{-1}).

3.1.2. Effect of pH and current density on captopril removal

The treatment of 0.230 mM captopril in the three aqueous matrices was extended to neutral pH 7.0 and alkaline conditions (pH 9.0). Fig. S1a-c and Fig. S2a-c depict the corresponding time course of the normalized drug concentration removals by AO-H_2O_2 with BDD, Pt and IrO_2, at j = 33.3 mA cm^2. The excellent pseudo-first-order kinetic analysis of such trends is shown in Fig. S1d-f and Fig. S2d-f, respectively. These results corroborate the upgrading of the oxidation ability of AO-H_2O_2 in the sequence: IrO_2 < Pt < BDD, as was found at pH 3.0. This

means that BDD stands out as the most powerful anode, owing to the action of active chlorine and/or BDD(•OH). The role of the former oxidant was evidenced in the two chloride media, with much greater k_1-values compared to those in sulfate medium (see Table 1). Table 1 also highlights a decrease of k_1 as pH was increased, regardless of the matrix or the anode. This phenomenon was less significant in sulfate medium, remaining even invariable using IrO_2. The k_1 drop upon pH change from pH 3.0 to 9.0 was more evident in the two chloride media, especially in the case of synthetic urine, undergoing a 0.41-fold, 0.32-fold and 0.27-fold decrease using BDD, Pt and IrO_2, respectively. The larger influence of pH in these matrices can be accounted for by the gradual conversion of HClO into ClO^- (pK_a = 7.45) and the loss of oxidation ability of the M(•OH) [5,15]. The progressive formation of the weak oxidant ClO^-, with E^o = 0.89 V/SHE [3], promoted a larger inhibition of captopril removal.

The lower performance of AO-H_2O_2 upon pH increase also caused a poorer TOC removal, with the concomitant rise in EC_{TOC} (see Table 1). In this regards, another interesting finding from Table 1 is the gradual mineralization enhancement as the organic load of the matrix was increased. For example, at pH 7.0, the use of BDD at j = 33.3 mA cm^{-2} yielded a mineralization percentage of 12% at 120 min in sulfate medium (initial TOC = 25 mg C L^{-1}), 20% at 120 min in urban wastewater (initial TOC = 37 mg C L^{-1}) and 23% at 60 min in synthetic urine (initial TOC: 745 mg C L^{-1}). This represents an increasing loss of 3.0, 7.4 and 171.4 mg C L^{-1} of TOC, accounting for decreasing EC_{TOC} values of 5.28, 1.26 and 0.055 kWh (g TOC)$^{-1}$, respectively. These results reveal the partial destruction of the 12 mg L^{-1} TOC present in the urban wastewater associated to the natural organic matter (NOM), which includes humic, fulvic and tannic acids [7,29]. Furthermore, there is clear evidence of partial mineralization of the aliphatic urea and the two heterocyclic compounds, uric acid and creatinine, of the synthetic urine matrix. In the literature, the destruction of urea by AO with Pt in sulfate medium has been reported [41], but the removal of uric acid and creatinine has not been described yet. On the other hand,

Cotillas et al. [38] have reported a large mineralization of synthetic urine matrices thanks to the action of HClO formed at a BDD anode.

The current density is a key parameter that modulates the generation of oxidizing agents in the AO-H_2O_2 process. A higher degradation rate is expected with raising *j*, in agreement with the increasing rate of the electrode reactions (1), (3) and (8), thus ending in a greater quantity of H_2O_2, M($^{\bullet}$OH) and HClO, respectively [3,29]. This effect was assessed in the three matrices at pH 7.0 using the BDD anode. Fig. 2a-c confirm the enhancement of captopril removal upon rise of *j* from 16.7 to 66.7 mA cm^{-2}. This trend was less substantial in urine, probably by the dominant role of active chlorine due to its higher Cl^- content. The drug always obeyed a pseudo-first-order reaction, as corroborated from the good fittings shown in Fig. 2d-f. The behavior was confirmed from the higher k_1-value and percentage of TOC removal determined as *j* was increased, as listed in Table 1. However, note that the EC_{TOC} values also became progressively higher, owing to the greater E_{cell}, which is detrimental if the cost must be minimized. Additionally, the increase in rate of parasitic reactions of the oxidants, as detailed below, caused a relatively smaller $\triangle(TOC)_{exp}$ with the consequent negative impact on EC_{TOC}.

In all matrices, the degradation rate also became lower as *j* rose. Thus, the k_1 increase was 1.9-fold in pure sulfate, 3.0-fold in wastewater and 1.8-fold in urine upon a fourfold rise of *j*, from 16.7 to 66.7 mA cm^{-2} (see Table 1). This disagreement can be related to the gradually larger extent to which parasitic reactions occurred. In the case of BDD($^{\bullet}$OH), these reactions include its immediate conversion to O_2 gas and H_2O_2 because of the lack of drug molecules on the anode surface, and its reaction with H_2O_2 to produce the weaker oxidant $HO_2^{\bullet}$ [7,10-12]. Regarding active chlorine, it can be mainly undergo oxidation to yield ClO_2^-, ClO_3^- and ClO_4^- ions [3,29]. From these findings, it is evident that a higher *j* causes a larger destruction of the organic matter, although at the expense of current efficiency.

3.1.3. Inorganic ions formed during captopril treatment in synthetic urine at neutral pH

To corroborate the aforementioned destruction of the organic components of the urine matrix, the inorganic species generated with each anode at the different pH values were analyzed. Fig. 3a-c depict the concentration of nitrogenated species detected after 60 min at j = 33.3 mA cm^{-2}. A large amount of NO_3^- and NH_4^+ ions was accumulated under all conditions, whereas NO_2^- ion only appeared at pH 7.0 and 9.0 and its concentration was smaller. The NO_2^- accumulation was always greater at pH 7.0, increased in the order: IrO_2 < Pt < BDD, and attained a maximum value of 7.6 mg L^{-1} (0.16 mM N). This tendency agrees with the higher oxidation ability of BDD to destroy the *N*-compounds. The same sequence can be observed for the NO_3^- ion with the three anodes at pH 3.0, dropping from 63.2 mg L^{-1} (1.02 mM N) with BDD to 34.9 mg L^{-1} (0.56 mM N) with IrO_2. In contrast, similar NO_3^- concentrations were found at pH 7.0 and 9.0 using BDD and IrO_2, being slightly lower with Pt. Conversely, in the case of NH_4^+ ion, higher concentrations were always obtained using Pt, reaching the greatest concentration of 42.6 mg L^{-1} (2.37 mM N). Note that the N content associated to captopril spiked into the synthetic urine (i.e., 0.230 mM) was much lower than that corresponding to the sum of accumulated NO_3^- and NH_4^+, revealing that the two latter ions pre-eminently proceeded from the destruction of urea, uric acid and creatinine, the *N*-components of the synthetic urine.

The active chlorine concentration accumulated in treated urine during the above trials is depicted in Fig. 3d. The greatest accumulation was obtained using Pt, regardless of the pH tested, suggesting that this anode fostered reaction (8). Its maximum concentration was 6.4 mg L^{-1} at pH 3.0. The attack of such a high amount of active chlorine on the *N*-compounds could justify the prevalence of NH_4^+ ion, alongside the lower production of NO_3^- ion at pH 7.0 and 9.0, as compared to BDD and IrO_2 (see Fig. 3a-c).

3.2. SPEF treatment of captopril solutions

3.2.1. H_2O_2 accumulation in the solar pre-pilot flow plant

The ability of the flow plant to accumulate H_2O_2 electrogenerated with a Pt/air-diffusion cell was first assessed by treating 2.5 L of 0.050 M Na_2SO_4 solutions at pH 3.0 and 35 ºC under AO-H_2O_2 conditions at different *j* values. Fig. S3a shows a progressive increase of the H_2O_2 concentration at each given *j*, attaining a final value of 4.3, 9.5 and 14.1 mM at 10, 30 and 50 mA cm^{-2}, respectively. For each trial, the current efficiency for H_2O_2 accumulation calculated from Faraday's law decreased over time. At j = 30 mA cm^{-2}, for instance, the efficiency was 69.5% at 60 min, 60.7% at 150 min and 42.4% at 300 min. This gradual decay can be related to the acceleration of H_2O_2 destruction from reaction (2), which results from the use of an undivided cell [15]. Fig. S3b also shows a decrease of current efficiency as *j* became higher, varying from 57.8% at 10 mA cm^{-2} to 34.9% at j = 50 mA cm^{-2}. The increase of *j* accelerated all electrode reactions, thereby promoting the H_2O_2 production via reaction (1) but comparatively favoring its destruction via reaction (2), finally causing the efficiency drop shown in Fig. S3b.

The H_2O_2 accumulation was also determined under EF and SPEF conditions, at j = 50 mA cm^{-2}, in the presence of 0.50 mM Fe^{2+} as catalyst. Fig. S3a shows that, in EF, the H_2O_2 content decayed strongly and only reached 3.1 mM at 300 min (7.7% of current efficiency). This means that, apart from the H_2O_2 loss via reaction (2), this compound was more largely removed via Fenton's reaction (4), with the consequent production of $^{\bullet}OH$ that could upgrade the water treatment. A higher drop of H_2O_2 concentration occurred under SPEF conditions, with a final value of 1.4 mM (3.5% of current efficiency). This is due to the acceleration of Fenton's reaction (4) resulting from Fe^{2+} regeneration via reaction (5). Based on all these results, EF and SPEF processes can be employed for the oxidation of organic pollutants and their by-products.

3.2.2. Captopril removal by different EAOPs in sulfate medium

Solutions with 0.230 mM captopril (i.e., 25 mg C L^{-1} TOC) and 0.050 M Na_2SO_4 at pH 3.0 were comparatively treated by AO-H_2O_2, EF and SPEF processes using the pre-pilot flow plant,

316 at j = 50 mA cm^{-2}. A Pt anode was utilized as example of active anodes, which are less expensive
317 than the non-active BDD and show similar degradation efficiency in SPEF [7,21,29]. The
318 Fenton-based EAOPs were made in the presence of 0.50 mM Fe^{2+} since this is the optimum
319 content found for similar treatments of aromatic pollutants with an air-diffusion cathode [7].
320 The value of pH change remained quite constant throughout these trials.

321 The decay of normalized drug concentration with electrolysis time is presented in Fig. 4a.
322 The degradation of captopril by AO-H_2O_2 process was very slow, with a disappearance as low
323 as 36% at 30 min. This confirms the very low oxidation power of electrogenerated H_2O_2 and
324 Pt($^{\bullet}$OH) formed from reaction (3) to destroy the drug, as found at small scale. In contrast, a
325 much faster captopril removal was provided by EF, with a complete drug removal in about 20
326 min. This is an evidence of the very effective attack of free $^{\bullet}$OH produced via Fenton's reaction
327 (4) in all the volume, being a good alternative to hydroxyl radicals confined within the anode
328 vicinity. The degradation rate was slightly increased in the SPEF process, with total removal in
329 only 15 min thanks to the greater generation of $^{\bullet}$OH upon photoreduction reaction (5). These
330 results agree with the behavior described for H_2O_2 accumulation in Fig. S3a.

331 The exponential concentration decays shown in Fig. 4a were analyzed assuming a pseudo-
332 first-order kinetics for captopril removal. Excellent linear regressions were obtained, as can be
333 seen in Fig. 4b. This means that also in Fenton-based EAOPs a steady quantity of oxidizing
334 agents was generated within the range of conditions tested. Table 2 collects the k_1-values
335 obtained, always with R^2 > 0.99. The lowest k_1-value was determined in the less powerful
336 process (i.e., AO-H_2O_2), which experienced a 22-fold and 30-fold increase in EF and SPEF,
337 respectively. The impressive rise confirms the relevance of homogeneous $^{\bullet}$OH formed from
338 reaction (4) and/or (5).

339 The TOC abatement in the above trials was measured for 300 min (data not shown). The
340 final percentages of TOC removal are listed in Table 2. As can be seen, the mineralization

degree increased in accordance with the oxidation power of the EAOPs, i.e., AO-H_2O_2 < EF < SPEF. Note the very low TOC decay achieved by AO-H_2O_2, as expected from the very slow drug disappearance (see Fig. 4a). Surprisingly, TOC was only reduced by 25% (6.2 mg C L^{-1} TOC) in SPEF, suggesting that the by-products formed were pre-eminently oxidized by homogeneous •OH, but with a very small generation of photoactive Fe(III) complexes that were rapidly removed via reaction (6). This behavior has not been observed for aromatic and heteroaromatic pollutants, whose mineralization by SPEF can be almost complete and fast because of the occurrence of such active complexes that are quickly transformed into CO_2 [1,15,22]. The corresponding EC_{TOC} values calculated at 300 min were as high as 30.1 kWh (g TOC)$^{-1}$ in AO-H_2O_2, being much smaller in EF (5.9-fold) and SPEF (8.9-fold) (see Table 2).

3.2.3. Effect of experimental variables on the SPEF process in sulfate medium

The influence of key experimental variables such as applied *j* and drug concentration on the performance of the SPEF process was examined. Fig. 5 depicts the gradual enhancement of captopril degradation when *j* was increased from 10 to 50 mA cm^{-2} to treat 0.230 mM drug solutions, owing to the larger presence of •OH resulting from the acceleration of H_2O_2 electrogeneration. A change from 10 to 30 and 50 mA cm^{-2} led to a shorter time span of 60, 40 and 15 min for total removal. The inset panel of Fig. 5 presents the good linear profiles obtained for these concentration abatements. The resulting k_1-values, shown in Table 2, evidence that the change from 30 to 50 mA cm^{-2} was beneficial, as deduced from the 3.3-fold increase of k_1. Therefore, at 50 mA cm^{-2}, the attack of •OH on the drug was more favored than the parasitic reactions mentioned above. The percentage of TOC removal at 300 min was also upgraded, from 16% at j = 10 mA cm^{-2} to 25% at j = 50 mA cm^{-2}, as shown in Table 2. In turn, this table reveals a strong increase of EC_{TOC} at higher *j*, resulting from the higher *j* and E_{cell}.

The influence of drug content was studied from 0.100 to 0.460 mM (from 11 to 50 mg C L^{-1} TOC) in 0.050 M Na_2SO_4 solutions, at pH 3.0 and j = 50 mA cm^{-2}. The rise of the initial

concentration led to a longer electrolysis time for total removal. Fig. 6 highlights that captopril disappeared from the medium at increasing time, from 5 min at 0.100 mM to 30 min at 0.460 mM. A positive feature was that the degradation process became more efficient. Thus, after 5-6 min, a concentration of 0.100 mM was removed from the less concentrated solution, whereas 0.212 and 0.314 mM were removed from the solutions initially containing 0.230 and 0.460 mM, respectively. This is correlated with the enhanced oxidation power of the system thanks to the larger number of reactive events between captopril molecules and the oxidants. Obviously, this tendency is opposite to that of k_1, determined from the excellent linear regressions presented in the inset panel of Fig. 6. The data of Table 2 show the drop of the k_1-value from 1.128 min^{-1} at 0.100 mM to 0.186 min^{-1} at 0.460 mM, in agreement with the longer time required for total drug abatement. This fact is also deduced from Table 2 considering the percentage of TOC removed at 300 min in SPEF, since it decayed significantly from 33% to 19% when treating 0.100 and 0.460 Mm, respectively. Nevertheless, the amount of TOC abated varied from 3.6 to 9.5 mg C L^{-1}, in agreement with a greater mineralization current efficiency. This trend was reflected in the EC_{TOC} values, which were 2.7-fold lower at 0.460 mM as compared to 0.100 mM, attaining a minimal of 2.27 kWh $(g\ TOC)^{-1}$ (see Table 2). These findings demonstrate that the SPEF treatment was more cost-effective when the solutions were more contaminated.

3.2.4. Effect of the aqueous matrix on captopril removal performance

Once clarified the behavior of the SPEF process in sulfate medium at pH 3.0, the study was extended to aqueous matrices where captopril has been detected, namely urban wastewater and urine. The latter medium was simulated as described in subsection 2.2 (matrices called urine 1, urine 2 and urine 3).

The urban wastewater contained 12 mg C L^{-1} TOC. Captopril was spiked at a concentration of 0.230 mM into 2.5 L of this matrix, yielding 37 mg C L^{-1} TOC, and the resulting solution was adjusted to pH 3.0 with H_2SO_4. After addition of Fe^{2+} (0.50 mM), it was treated by SPEF

391 in the pre-pilot flow plant, at j = 50 mA cm^{-2}. Fig. 7 shows a rapid disappearance of the drug in
392 only 15 min, a time analogous to that needed in sulfate medium (see Fig. 4). From the pseudo-
393 first-order kinetic analysis depicted in the inset panel of Fig. 7, a higher k_1-value of 0.551 (vs.
394 0.452 min^{-1}) was obtained in wastewater (see Table 2). Since the natural organic components
395 of this matrix are supposed to partially scavenge the •OH [7], a deceleration of the drug decay
396 was presumed, but the opposite behavior was observed. This can be accounted for by the
397 generation of active chlorine (HClO) in SPEF. The simultaneous degradation of captopril by
398 both oxidants (•OH and HClO) in urban wastewater enhanced the SPEF performance. The
399 existence of these oxidants also justified the higher percentage of TOC removal (28%, i.e., 10.4
400 mg C L^{-1} of TOC) found in urban wastewater as compared to 6.2 mg C L^{-1} determined in sulfate
401 medium, which can be ascribed to the partial mineralization of NOM. Note also in Table 2 the
402 much higher EC_{TOC} value for the trial in wastewater, because of the much greater E_{cell} resulting
403 from its smaller conductivity.

404 Captopril was also spiked into each synthetic urine matrix at a concentration of 0.230 mM,
405 the solution pH was adjusted to pH 3.0 and Fe^{2+} (0.50 mM) was added as catalyst. Fig. 7 depicts
406 the change of normalized drug concentration with electrolysis time for the assays performed at
407 j = 50 mA cm^{-2}. As expected, the larger competition between captopril and a gradually higher
408 quantity of organic components in the urine matrix caused a deceleration of drug degradation.
409 Anyway, overall captopril abatement was always achieved, requiring 15, 20 and 30 min using
410 urine 1, 2 and 3, respectively. The content of oxidants remained constant in each matrix, which
411 explains the good pseudo-first-order kinetic analysis of the concentration decays (inset panel of
412 Fig. 7). The corresponding k_1-values given in Table 2 dropped significantly, about 50% when
413 moving from the diluted urine 1 to the most concentrated urine 3.

414 The concomitant oxidation of the organic components of the urine matrices was also
415 observed when monitoring their TOC abatement. Fig. 8a shows a rapid mineralization with

TOC reduction by 70% using urine 1 (205 mg C L^{-1} of initial TOC, including the 25 mg C L^{-1} of captopril), which decreased down to a 44% using urine 2 (385 mg C L^{-1}) and to a 26% using urine 3 (745 mg C L^{-1}). Despite this, increasing quantities, i.e., 143, 169 and 194 mg C L^{-1} of TOC, were removed, confirming the suitability of the EAOPs to efficiently treat concentrated solutions. These results clearly evidence that the aliphatic urea and the heterocyclic molecules of the aqueous matrices can be largely mineralized by the SPEF process.

The EC_{TOC} values decreased as the organic load in the urine matrix became higher. This trend can be seen inferred from the EC_{TOC}-time plots of Fig. 8b as well as from the final values listed in Table 2, because similar E_{cell} values between 10.1 and 10.7 V were measured in these trials. Fig. 8b also shows an atypical profile of EC_{TOC}. During the treatment of aromatic an heteroaromatic pollutants, this parameter always grows as the electrolysis progresses, due to the gradual formation of more recalcitrant by-products [1,5]. The opposite tendency can be observed in this figure, where EC_{TOC} always decreased as the electrolysis was prolonged, informing about the gradual production of less refractory by-products. Such species could be short-linear aliphatic acids arising from the destruction of uric acid and creatinine, further giving rise to photoactive Fe(III)-carboxylate complexes that are more easily photolyzed by sunlight. In the next subsection, the main reaction by-products are determined.

3.2.5. Identification of main by-products of captopril

Table S1 collects the names, chemical structure and characteristics of 6 main by-products detected by GC-MS after 10 min of SPEF treatment of a 0.230 mM drug solution with 0.050 M Na_2SO_4 at pH 3.0 using the solar pre-pilot flow plant at j = 50 mA cm^{-2}. Considering these compounds, a plausible pathway for captopril (**1**) degradation is proposed in Fig. 9, where the main oxidant is the homogeneous $^{\bullet}OH$ formed from Fenton's reaction (4), with the important contribution of the photoreduction reaction (5). It should be noted that the four carboxylic acids (compounds **4** to **7**) are either free or in the form of complexes with Fe(III) [5,7,15], but most

441 of them are expected to possess a very low photoactivity, as deduced from the low TOC removal
442 achieved under these conditions (see Table 2). Although the route of Fig. 9 is proposed for the
443 SPEF process, it could be extended to AO-H_2O_2 and EF since Pt(•OH) and/or •OH are the main
444 oxidizing agents as well.

445 The pathway of Fig. 9 is initiated by the attack of •OH over **1** causing its decarboxylation,
446 demethylation and loss of a sulfonylmethyl molecule to yield **2**, which is further oxidized to the
447 pyrrolidone **3**. The subsequent cleavage of the pyrrolidine moiety at the N(1)-C(5) bond
448 originates the acid **4**, which is then oxidized and broken to form the acids **5** and **6**. Finally, the
449 oxidation of these two acids leads to acid **7**. It should be mentioned that acid **7** is very stable to
450 the attack of •OH and must be mineralized to CO_2 via oxidation to oxalic and formic acids as
451 intermediates [5,15].

452 **4. Conclusions**

453 The effectiveness of the AO-H_2O_2 process with an air-diffusion cathode to degrade the
454 heterocyclic drug captopril at pH 3.0-9.0 was greater in urban wastewater and urine, as
455 compared to that observed in sulfate, owing to combined action of M(•OH) and active chlorine.
456 BDD anode ensured the highest performance, and in all media the oxidation power decreased
457 at higher pH. The rise of *j* accelerated the degradation but at the expense of current efficiency.
458 A low mineralization was achieved, regardless of the matrix and the anode, being higher in
459 urine. The larger accumulation of NO_3^- and NH_4^+ ions in urine was related to the destruction
460 of its *N*-compounds. The SPEF process with a Pt/air-diffusion cell clearly outperformed the
461 AO-H_2O_2 and EF treatments, as a result of the effective production of •OH. However, the
462 mineralization tended to be low, suggesting a small production of photoactive Fe(III)
463 complexes with organic molecules. The oxidation power was higher as the initial solution was
464 more concentrated. The degradation and mineralization in urban wastewater was slightly

accelerated as compared to those in sulfate medium because of the parallel oxidation with active chlorine, but its low conductivity derived in a much higher EC_{TOC}. Total drug decay was also feasible in urine, showing a larger mineralization with lower EC_{TOC} values. Two heterocyclic derivatives and four linear acids were identified as by-products.

Acknowledgements

Financial support from project CTQ2016-78616-R (AEI/FEDER, EU), as well as from the Coordenação de Aperfeiçoamento de Pessoal de Nível Superior - Brasil (CAPES) - Finance Code 001, is acknowledged. A.J. dos Santos acknowledges funding from CAPES (Brazil) through program "Pesquisa Pós-doutoral no Exterior" number 88881.172332/2018-01.

References

[1] E. Brillas, A review on the degradation of organic pollutants in waters by UV photoelectro-Fenton and solar photoelectro-Fenton, J. Braz. Chem. Soc. 25 (2014) 393-417.

[2] I. Salmerón, K.V. Plakas, I. Sirés, I. Oller, M.I. Maldonado, A.J. Karabelas, S. Malato, Optimization of electrocatalytic H_2O_2 production at pilot plant scale for solar-assisted water treatment, Appl. Catal. B: Environ. 242 (2019) 327-336.

[3] M.F. Murrieta, I. Sirés, E. Brillas, J.L. Nava, Mineralization of Acid Red 1 azo dye by solar photoelectro-Fenton-like process using electrogenerated HClO and photoregenerated Fe(II), Chemosphere 246 (2020) 125697.

[4] M.A. Oturan, J.J. Aaron, Advanced oxidation processes in water/wastewater treatment: principles and applications. A review. Crit. Rev. Environ. Sci. Technol. 44 (2014) 2577-2641.

[5] C.A. Martínez-Huitle, M.A. Rodrigo, I. Sirés, O. Scialdone, Single and coupled electrochemical processes and reactors for the abatement of organic pollutants: A critical review, Chem. Rev. 115 (2015) 13362-13407.

[6] J. Vidal, C. Huilñir, R. Salazar, Removal of organic matter contained in slaughterhouse wastewater using a combination of anaerobic digestion and solar photoelectro-Fenton processes, Electrochim. Acta 210 (2016) 163-170.

[7] J.R. Steter, E. Brillas, I. Sirés, Solar photoelectro-Fenton treatment of a mixture of parabens spiked into secondary treated wastewater e□uent at low input current, Appl. Catal. B: Environ. 224 (2018) 410-418.

[8] D.R.V Guelfi, E. Brillas, F. Gozzi, A. Machulek Jr., S.C. de Oliveira, I. Sirés, Influence of electrolysis conditions on the treatment of herbicide bentazon using artificial UVA radiation and sunlight. Identification of oxidation products, J. Environ. Manage. 231 (2019) 213-221.

[9] S. Lanzalaco, I. Sirés, M.A. Sabatino, C. Dispenza, O. Scialdone, A. Galia, Synthesis of polymer nanogels by electro-Fenton process: investigation of the effect of main operation parameters, Electrochim. Acta 246 (2017) 812-822.

[10] A.J. dos Santos, C.A. Martínez-Huitle, I. Sirés, E. Brillas, Use of Pt and BDD anodes in the electrochemical advanced oxidation of Ponceau SS diazo dye in acidic sulfate medium, ChemElectroChem (2018) 685-693.

[11] A.J. dos Santos, I. Sirés, C.A. Martínez-Huitle, E. Brillas, Total mineralization of mixtures of Tartrazine, Ponceau SS and Direct Blue 71 azo dyes by solar photoelectro-Fenton in pre-pilot plant, Chemosphere 210 (2018) 1137-1144.

[12] M. Panizza, M.A. Oturan, Degradation of Alizarin Red by electro-Fenton process using a graphite-felt cathode, Electrochim. Acta 56 (2011) 7084-7087.

[13] A. El-Ghenymy, R.M. Rodríguez, E. Brillas, N. Oturan, M.A. Oturan, Electro-Fenton degradation of the antibiotic sulfanilamide with Pt/carbon-felt and BDD/carbon-felt cells. Kinetics, reaction intermediates, and toxicity assessment, Environ. Sci. Pollut. Res. 21 (2014) 8368-8378.

[14] O. Ganzenko, N. Oturan, I. Sirés, D. Huguenot, E.D. van Hullebusch, G. Esposito, M.A. Oturan, Fast and complete removal of the 5-fluorouracil drug from water by electro-Fenton oxidation, Environ. Chem. Lett. 16 (2018) 281-286.

[15] E. Brillas, I. Sirés, M.A. Oturan, Electro-Fenton process and related electrochemical technologies based on Fenton's reaction chemistry, Chem Rev 109 (2009) 6570-6631.

[16] M. Panizza, G. Cerisola, Direct and mediated anodic oxidation of organic pollutants, Chem. Rev. 109 (2009) 6541-6569.

[17] S. Lanzalaco, I. Sirés, A. Galia, M.A. Sabatino, C. Dispenza, O. Scialdone, Facile crosslinking of poly(vinylpyrrolidone) by electro-oxidation with IrO_2-based anode under potentiostatic conditions, J. Appl. Electrochem. 48 (2018) 1343-1352.

[18] E. do Vale-Júnior, A.J. dos Santos, D.R. da Silva, A.S. Fajardo, C.A. Martínez-Huitle, Electrochemical technologies for detecting and degrading benzoquinone using diamond films, ChemElectroChem 6 (2019) 4383-4390.

[19] F. Sopaj, M.A. Rodrigo, N. Oturan, F.I. Podvorica, J. Pinson, M.A Oturan, Influence of the anode materials on the electrochemical oxidation efficiency. Application to oxidative degradation of the pharmaceutical amoxicillin, Chem. Eng. J. 262 (2015) 286-294.

[20] S. Dbira, N. Bensalah, M.I. Ahmad, A. Bedoui, Electrochemical oxidation/disinfection of urine wastewaters with different anode materials, Materials 12 (2019) 1254.

[21] A. Thiam, I. Sirés, E. Brillas, Treatment of a mixture of food color additives (E122, E124 and E129) in different water matrices by UVA and solar photoelectro-Fenton, Water Res. 81 (2015) 178-187.

[22] A. Thiam, R. Salazar, Fenton-based electrochemical degradation of metolachlor in aqueous solution by means of BDD and Pt electrodes: influencing factors and reaction pathways, Environ. Sci. Pollut. Res. 26 (2019) 2580-2591.

[23] C. Espinoza, J. Romero, L. Villegas, L. Cornejo-Ponce, R. Salazar, Mineralization of the textile dye Acid Yellow 42 by solar photoelectro-Fenton in a lab-pilot plant, J. Hazard. Mater. 319 (2016) 24-33.

[24] A.S. Fajardo, A.J. dos Santos, E.C.T. de Araújo Costa, D.R. da Silva, C.A. Martínez-Huitle, Effect of anodic materials on solar photoelectro-Fenton process using a diazo dye as a model contaminant, Chemosphere 22 (2019) 880-889.

[25] L. Feng, E.D. van Hullebusch, M.A. Rodrigo, G. Esposito, M.A. Oturan, Removal of residual anti-inflammatory and analgesic pharmaceuticals from aqueous systems by electrochemical advanced oxidation processes. A review, Chem. Eng. J. 228 (2013) 944-964.

[26] E. Brillas, I. Sirés, Electrochemical removal of pharmaceuticals from water streams: reactivity elucidation by mass spectrometry, TRAC Trend. Anal. Chem. 70 (2015) 112-121.

[27] Y. Zhang, A. Wang, X. Tian, Z. Wen, H. Lv, D. Li, J. Li, Efficient mineralization of the antibiotic trimethoprim by solar assisted photoelectro-Fenton process driven by a photovoltaic cell, J. Hazard. Mater. 318 (2016) 319-328.

[28] G. Coria, T. Pérez, I. Sirés, E. Brillas, J.L. Nava, Abatement of the antibiotic levofloxacin in a solar photoelectro-Fenton flow plant: Modeling the dissolved organic carbon concentration-time relationship, Chemosphere 198 (2018) 174-181.

[29] C. Ridruejo, F. Centellas, P.L. Cabot, I. Sirés, E. Brillas, Electrochemical Fenton-based treatment of tetracaine in synthetic and urban wastewater using active and non-active anodes, Water Res. 128 (2018) 71-81.

[30] J.R.L.E. Freitas, F.J.O. Quintão, J.C.C. da Silva, S.Q.D. Silva, S.F. Aquino, R.J.C.F. Afonso, Characterisation of captopril photolysis and photocatalysis by-products in water by direct infusion, electrospray ionisation, high-resolution mass spectrometry and the assessment of their toxicities, Int. J. Environ. Anal. Chem. 97 (2017) 42-55.

[31] W.M. Mahmoud, K. Kümmerer, Captopril and its dimer captopril disulfide: Photodegradation, aerobic biodegradation and identification of transformation products by HPLC-UV and LC-ion trap-MS(n), Chemosphere 88 (2012) 1170-1177.

[32] R. Salgado, R. Marques, J.P. Noronha, J.T. Mexia, G. Carvalho, A. Oehmen, M.A.M. Reis, Assessing the diurnal variability of pharmaceutical and personal care products in a full-scale activated sludge plant, Environ. Pollut. 159 (2011) 2359-2367.

[33] Y. Chen, X. Xi, G. Yu, Q. Cao, B. Wang, F. Vince, Y. Hong, Pharmaceutical compounds in aquatic environment in China: locally screening and environmental risk assessment, Front. Environ. Sci. Eng. 9 (2015) 394-401.

[34] M.J.A. Cortes-Diaz, J. Rodríguez-Flores, G. Castañeda-Peñalvo, M. Galar-Martínez, H. Islas-Flores, O. Dublán-García, L.M. Gómez-Oliván, Sublethal effects induced by captopril on *Cyprinus carpio* as determined by oxidative stress biomarker, Sci. Total Environ. 605-606 (2017) 811-823.

[35] G.P. Kapungu, G. Rukweza, T. Tran, W. Mbiya, R. Adigun, P. Ndungu, B. Martincigh, R.H. Simoyi, Oxyhalogen−sulfur chemistry: kinetics and mechanism of oxidation of captopril by acidified bromate and aqueous bromine, J. Phys. Chem. A 117 (2013) 2704-2717.|

[36] A.M. Asiri, A.A.P. Khan, A. Khan, Spectroscopic investigation on kinetics and mechanistic aspects to electron-transfer process into quinolinium dichromate oxidation of a high blood pressure drug captopril in acidic medium, J. Mol. Liquids 203 (2015) 1-6.

[37] P. Du, H. Zhao, C. Liu, Q. Huang, H. Cao, Transformation and products of captopril with humic constituents during laccase-catalyzed oxidation: role of reactive intermediates, Water Res. 106 (2016) 488-495.

[38] S. Cotillas, E. Lacasa, C. Sáez, P. Cañizares, M.A. Rodrigo, Disinfection of urine by conductive-diamond electrochemical oxidation, Appl. Catal. B: Environ. 229 (2018) 63-70.

[39] C. Flox, J.A. Garrido, R.M. Rodríguez, P.L. Cabot, F. Centellas, C. Arias, E. Brillas, Mineralization of herbicide mecoprop by photoelectro-Fenton with UVA and solar light, Catal. Today 129 (2007) 29-36.

[40] F.J. Welcher, Standard Methods of Chemical Analysis, sixth ed, vol. 2, RE Krieger Publishing Co, Huntington, New York (Part B), 1975.

[41] C. Carlesi Jara, S. Di Giulio, D. Fino, P. Spinelli, Combined direct and indirect electroxidation of urea containing water, J. Appl. Electrochem. 38 (2008) 915-922.

Figure captions

Fig. 1. Normalized concentration decay vs. electrolysis time for the AO-H_2O_2 degradation of 0.230 mM captopril in 130 mL of (a) a 0.050 M Na_2SO_4 solution, (b) urban wastewater and (c) synthetic urine, at pH 3.0 and 35 ºC using a stirred undivided cell with different anodes (see legend in plot (a)) and a carbon-PTFE cathode, all of 3 cm^2 area, at a current density (*j*) of 33.3 mA cm^{-2}. The corresponding pseudo-first-order kinetic analysis is shown in plots (d), (e) and (f), respectively.

Fig. 2. Influence of current density (see legend in plot (a)) on the time course of the normalized concentration decay for the AO-H_2O_2 treatment of 0.230 mM captopril in 130 mL of (a) a 0.050 M Na_2SO_4 solution, (b) urban wastewater and (c) synthetic urine, at pH 7.0 and 35 ºC using a BDD/air-diffusion cell. The corresponding pseudo-first-order kinetic analysis is shown in plots (d), (e) and (f), respectively.

Fig. 3. Concentration of nitrogenated ions (see legend in plot (a)) after 60 min of AO-H_2O_2 treatment of 130 mL of 0.230 mM captopril in synthetic urine at different pH values using a (a) BDD, (b) Pt or (c) IrO_2 anode at j = 33.3 mA cm^{-2}. (d) Concentration of active chlorine determined under the same conditions.

Fig. 4. (a) Normalized concentration decay and (b) pseudo-first-order kinetic analysis for the treatment of 0.230 mM captopril in 2.5 L of a 0.050 M Na_2SO_4 solution at pH 3.0 and 35 ºC using a solar pre-pilot plant with a Pt/air-diffusion cell at j = 50 mA cm^{-2} and liquid flow rate of 180 L h^{-1}. Method: (●) AO-H_2O_2 (■) EF with 0.50 mM Fe^{2+} and (▲) SPEF with 0.50 mM Fe^{2+}.

Fig. 5. Effect of j on the normalized captopril concentration abatement for the SPEF treatment of 0.230 mM drug in 2.5 L of a 0.050 M Na_2SO_4 solution with 0.50 mM Fe^{2+} at pH 3.0 and 35 ºC using a solar pre-pilot flow plant with a Pt/air-diffusion cell at liquid flow rate of 180 L h^{-1}.

624 Current density: (◆) 10 mA cm^{-2}, (●) 30 mA cm^{-2} and (▲) 50 mA cm^{-2}. The pseudo-first-
625 order kinetic analysis of concentration decays is depicted in the inset panel.

626 **Fig. 6.** Influence of the initial captopril content on the change of its concentration with
627 electrolysis time for the SPEF treatment of 2.5 L of 0.050 M Na_2SO_4 solutions with 0.50 mM
628 Fe^{2+} at pH 3.0 and 35 ºC using a solar pre-pilot flow plant with a Pt/air-diffusion cell at j = 50
629 mA cm^{-2} and liquid flow rate of 180 L h^{-1}. Initial captopril content: (■) 0.100 mM, (▲) 0.230
630 mM and (▼) 0.460 mM. The inset panel presents the kinetic analysis of the concentration
631 decays assuming a pseudo-first-order reaction.

632 **Fig. 7.** Influence of the aqueous matrix on the normalized captopril concentration decay during
633 the SPEF treatment of 2.5 L of 0.230 mM drug solutions with 0.50 mM Fe^{2+} at pH 3.0 and 35
634 ºC using a solar pre-pilot flow plant with a Pt/air-diffusion cell at j = 50 mA cm^{-2} and liquid
635 flow rate of 180 L h^{-1}. Matrix: (▲) Urban wastewater, (■) urine 1 (13.9 mM urea + 0.073 mM
636 uric acid + 0.367 mM creatinine), (●) urine 2 (27.8 mM urea + 0.146 mM uric acid + 0.734
637 mM creatinine) and (▼) urine 3 (55.6 mM urea + 0.292 mM uric acid + 1.47 mM creatinine).
638 The inset panel shows the kinetic analysis of the above concentration decays assuming a
639 pseudo-first-order reaction.

640 **Fig. 8.** Time course of (a) TOC and (b) specific energy consumption per unit TOC mass for the
641 SPEF trials in (■) urine 1, (●) urine 2 and (▼) urine 3 shown in Fig. 7.

642 **Fig. 9**. Proposed route for captopril degradation by SPEF process in sulfate medium.

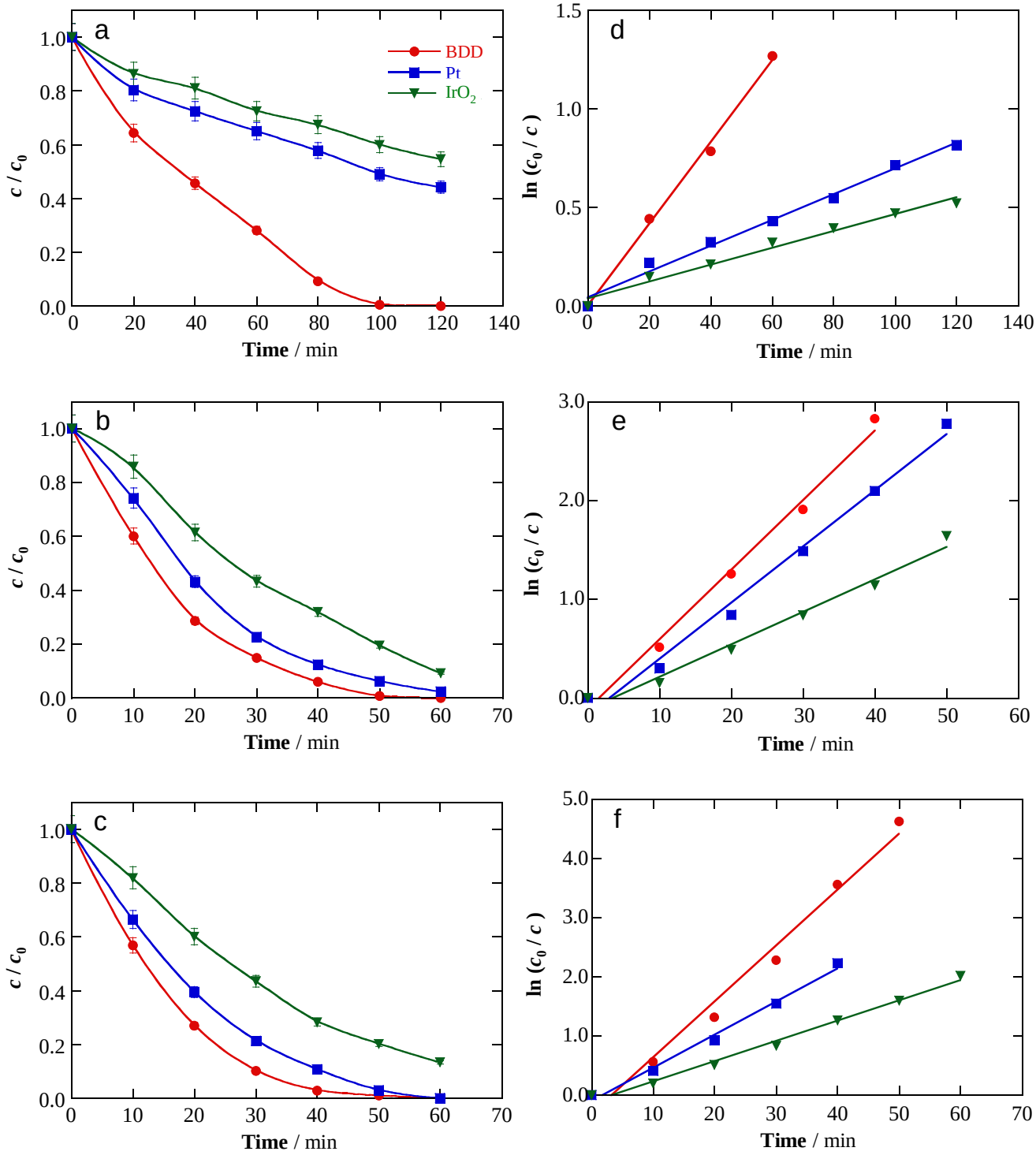
a
BDD
Pt
IrO2
c / c0
Time / min
d
ln (c0 / c)
Time / min
b
c / c0
Time / min
e
ln (c0 / c)
Time / min
c
c / c0
Time / min
f
ln (c0 / c)
Time / min

Fig. 1

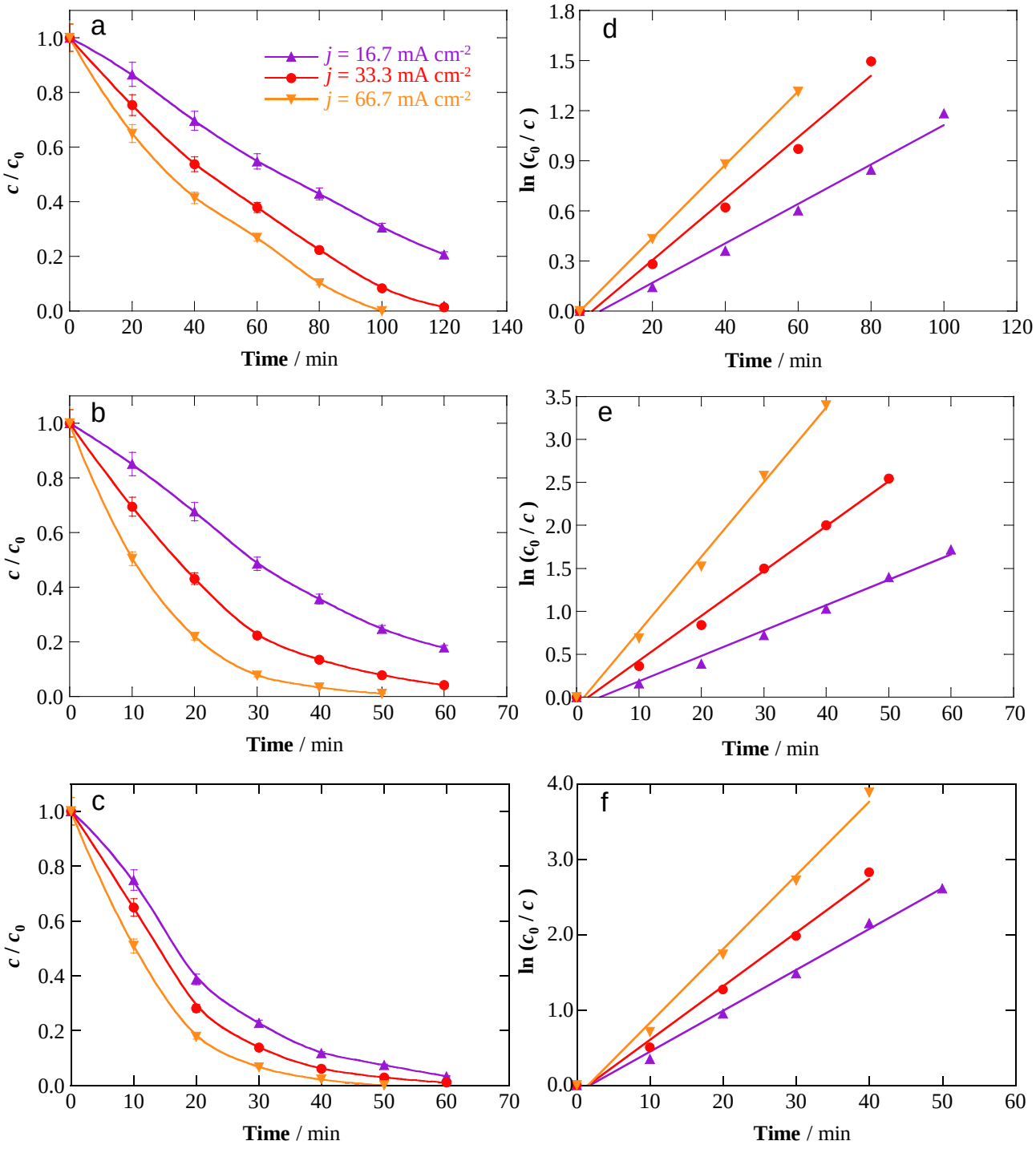
a
j = 16.7 mA cm-2
j = 33.3 mA cm-2
j = 66.7 mA cm-2
c / c0
Time / min
d
ln (c0 / c)
Time / min
b
c / c0
Time / min
e
ln (c0 / c)
Time / min
c
c / c0
Time / min
f
ln (c0 / c)
Time / min

Fig. 2

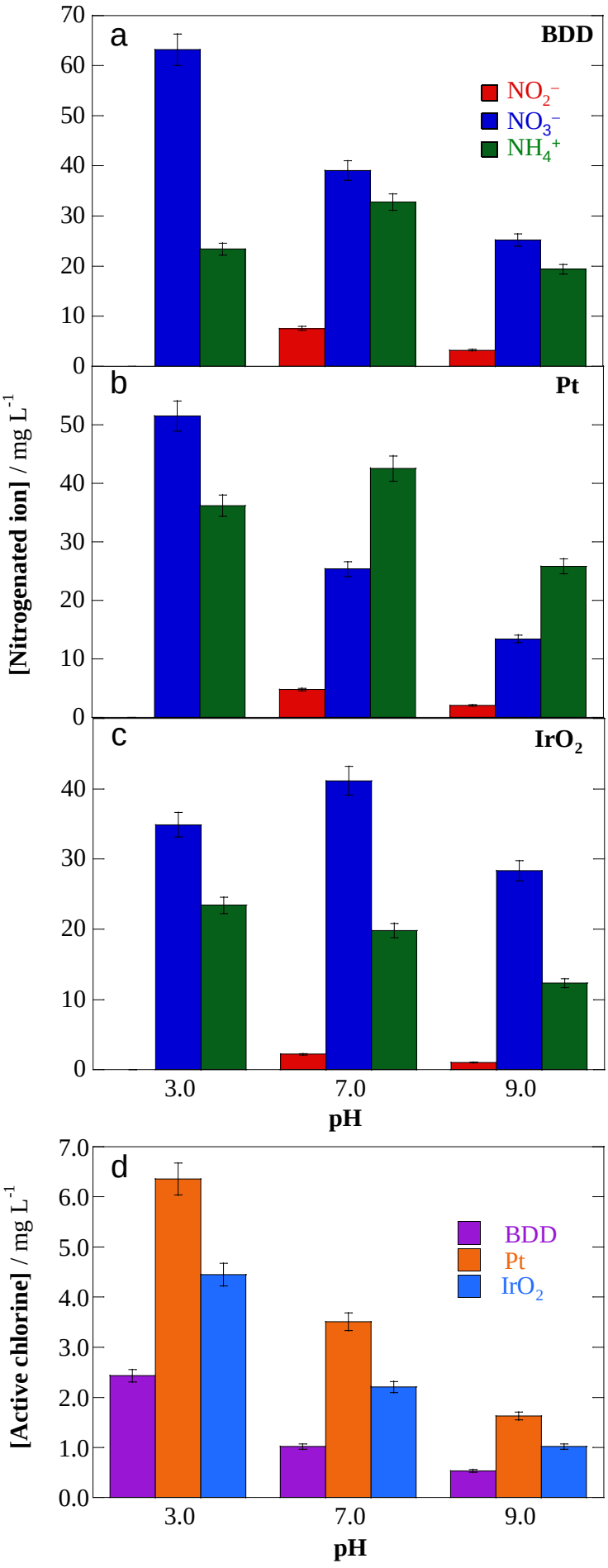
a
BDD
NO_2^-
NO_3^-
NH_4^+
b
Pt
c
IrO_2
[Nitrogenated ion] / mg L^{-1}
pH
d
BDD
Pt
IrO_2
[Active chlorine] / mg L^{-1}
pH

Fig. 3

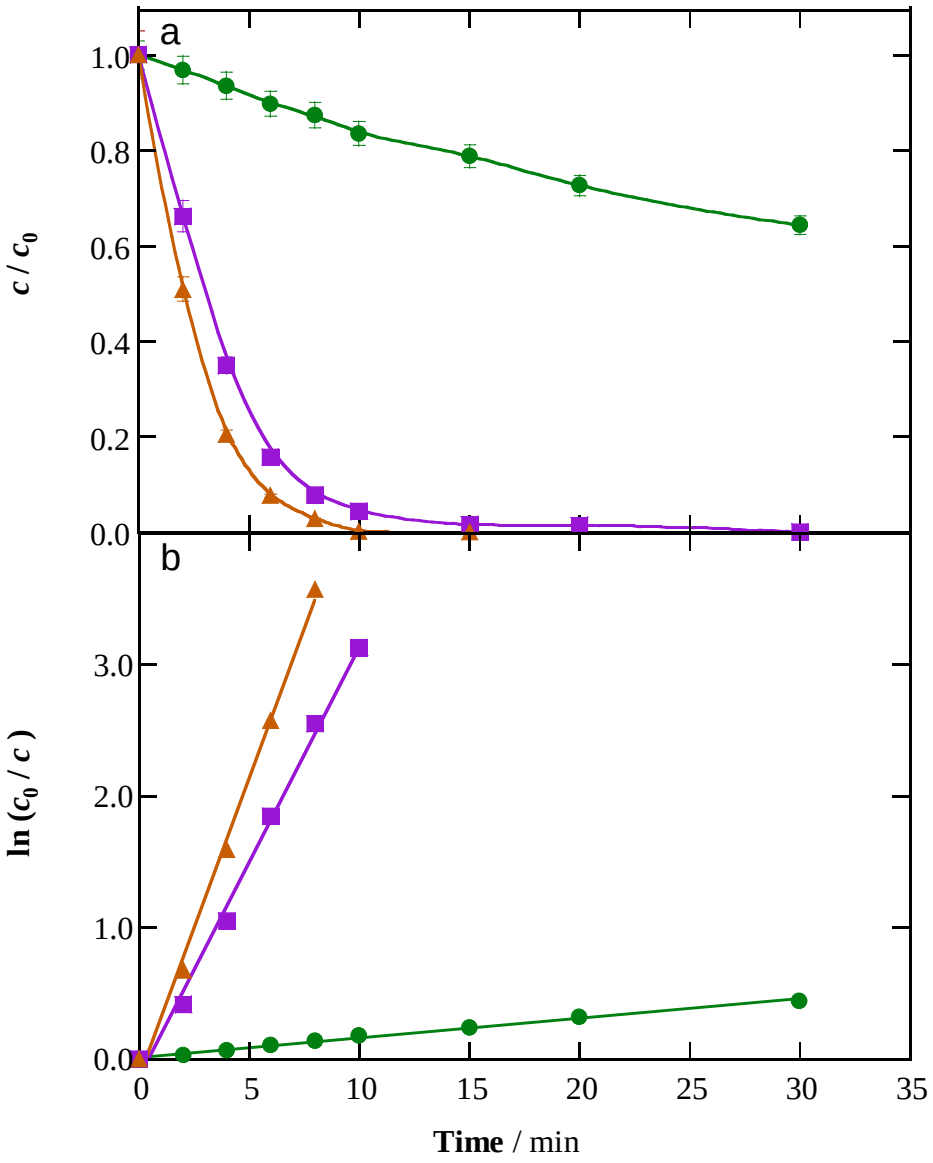
a
b
1.0
0.8
0.6
0.4
0.2
0.0
c / c0
3.0
2.0
1.0
0.0
ln (c0 / c)
0
5
10
15
20
25
30
35
Time / min

Fig. 4

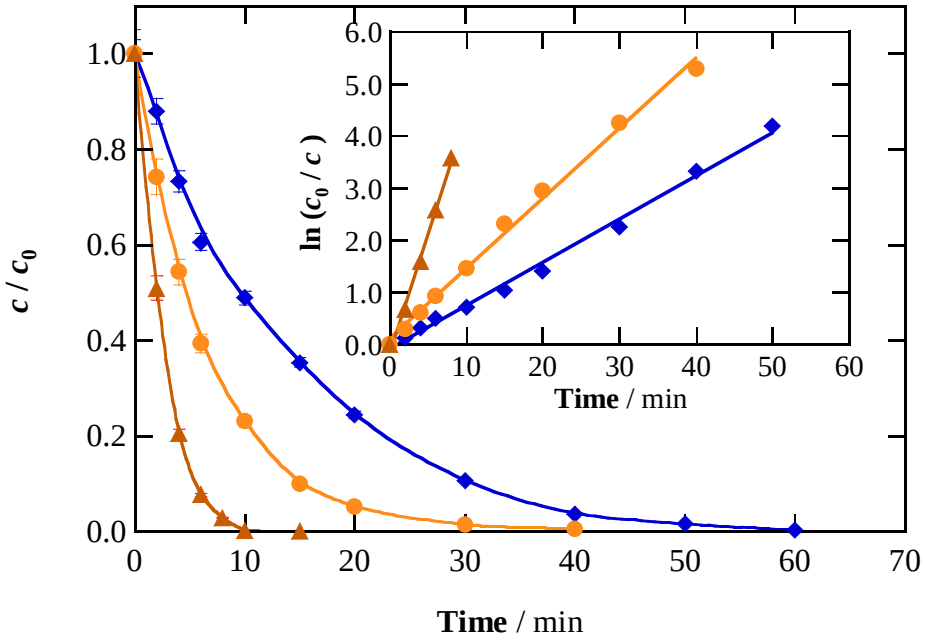

Fig. 5

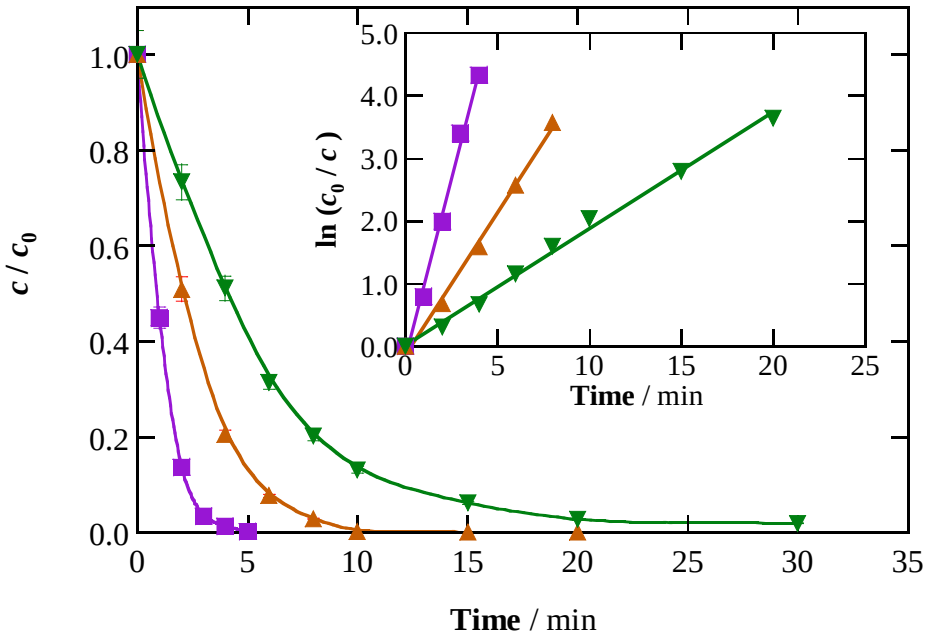

Fig. 6

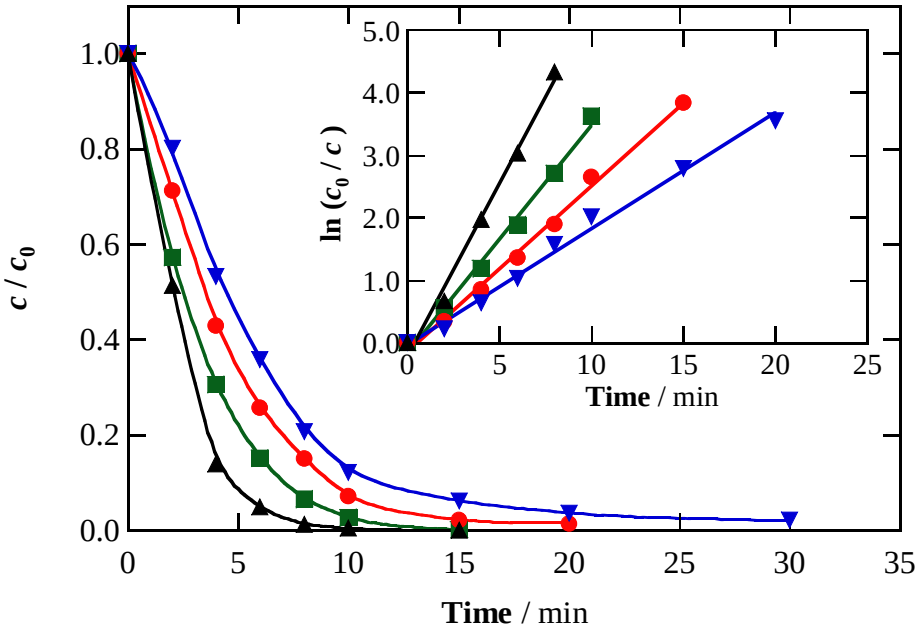
1.0
0.8
0.6
0.4
0.2
0.0
c / c0
0
5
10
15
20
25
30
35
Time / min
5.0
4.0
3.0
2.0
1.0
0.0
ln (c0 / c)
0
5
10
15
20
25
Time / min

Fig. 7

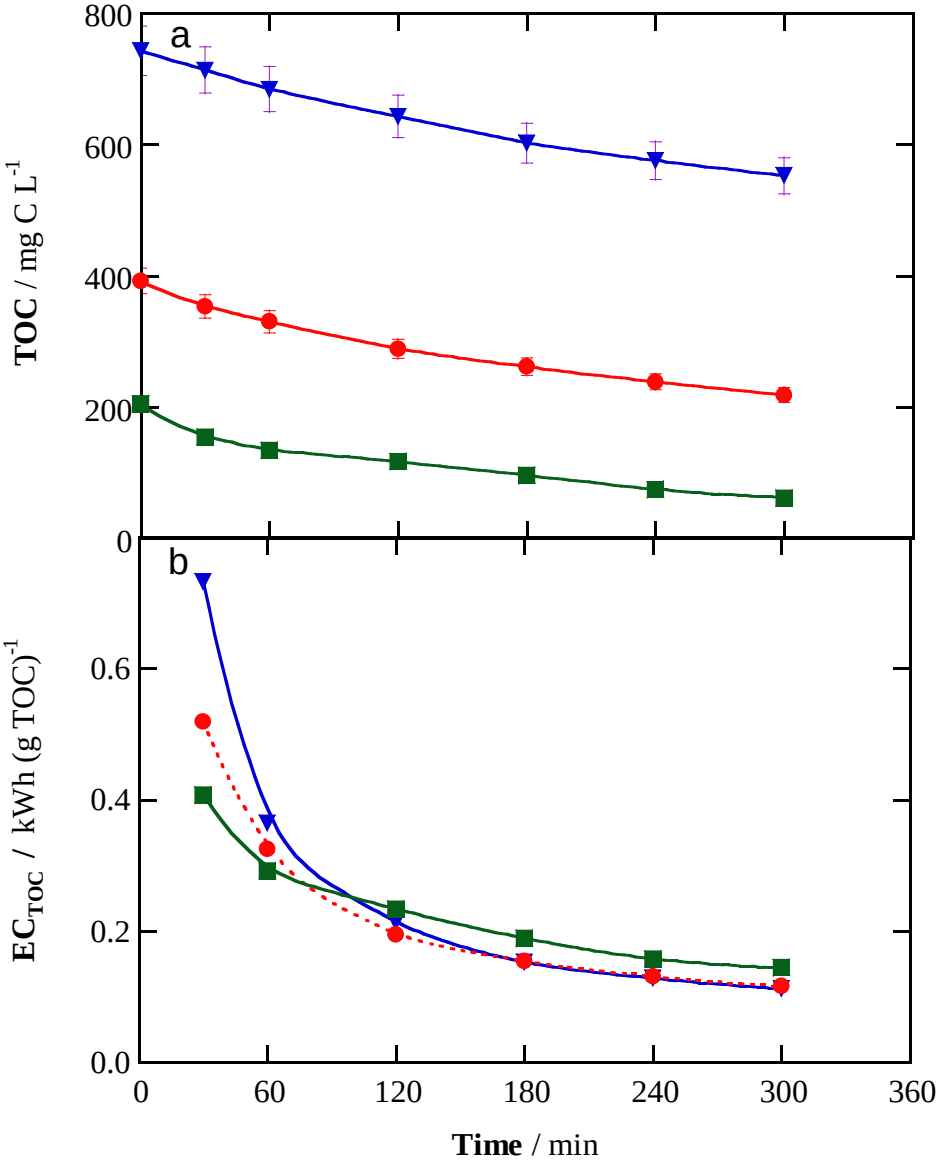
a
b
800
600
400
200
0
0.6
0.4
0.2
0.0
0
60
120
180
240
300
360
TOC / mg C L-1
ECTOC / kWh (g TOC)-1
Time / min

Fig. 8

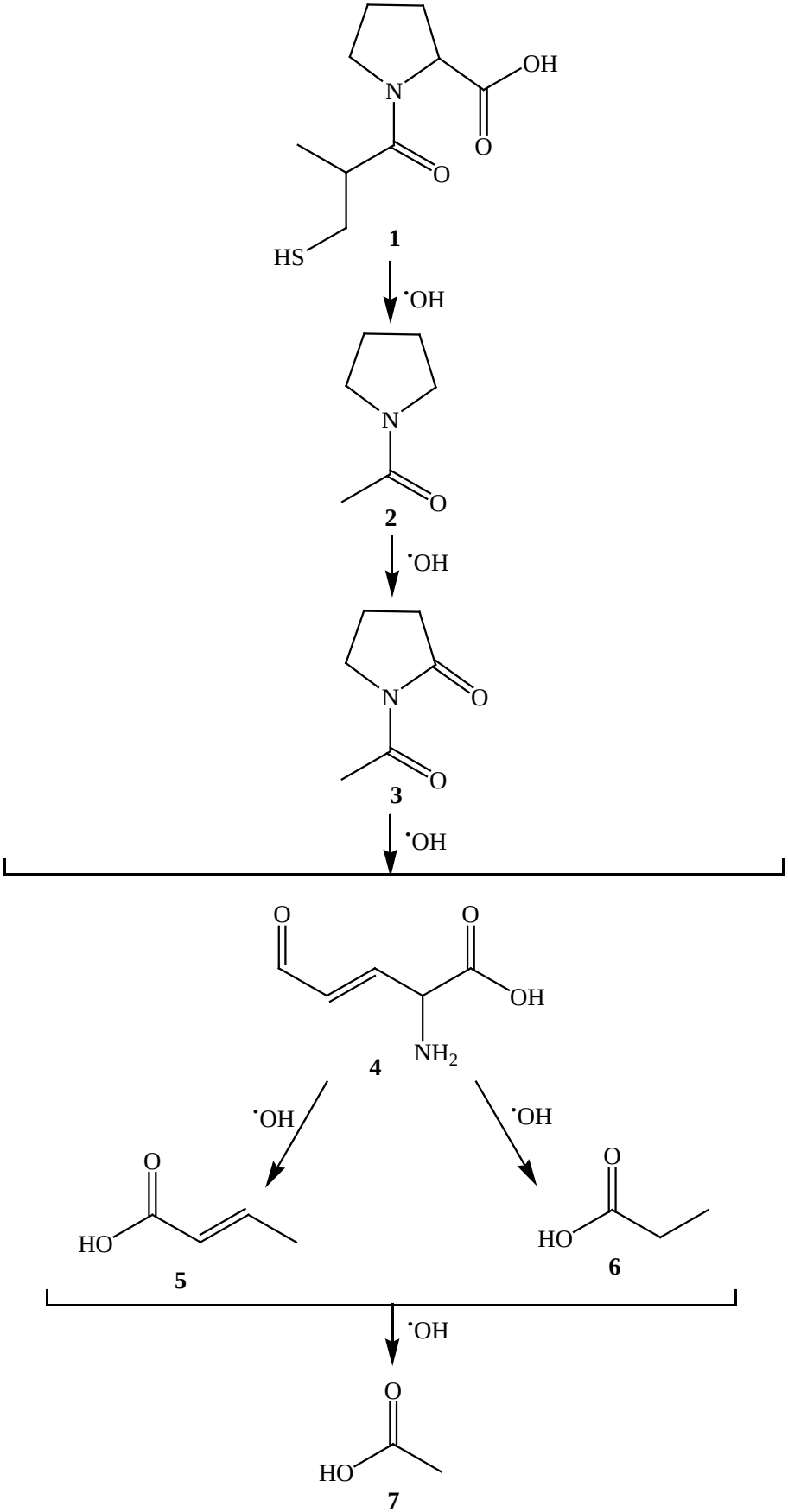

Fig. 9

Table 1.

Percentage of degradation, pseudo-first-order rate constant for captopril decay and its *R*-squared, and percentage of TOC removal and specific energy consumption per unit TOC mass for the treatment of 130 mL of a 0.230 mM drug solution in different aqueous matrices and varying pH values at 35 ºC using a stirred undivided cell with different anodes and an air-diffusion cathode.

Medium	pH	j (mA cm^{-2})	E_{cell} (V)	% Degradation (time (min))	k_1 (10^{-2} min^{-1})	R^2	% TOC removal	EC_{TOC} (kWh (g TOC)$^{-1}$)
BDD anode								
0.050 M Na_2SO_4 [a]	3.0	33.3	10.3	99 (120)	2.073	0.996	17	3.73
	7.0	16.7	6.2	80 (120)	1.181	0.986	6.9	2.76
		33.3	10.3	99 (120)	1.840	0.986	12	5.28
		66.7	13.9	100 (100)	2.196	0.998	23	7.41
	9.0	33.3	10.5	90 (120)	1.060	0.985	8.9	7.26
Urban wastewater [b]	3.0	33.3	12.1	96 (60)	6.684	0.982	- [d]	
	7.0	16.7	6.8	82 (60)	2.954	0.988	14	0.504
		33.3	12.1	96 (60)	5.229	0.994	20	1.26
		66.7	13.6	99 (50)	8.891	0.995	27	2.09
	9.0	33.3	10.5	94 (60)	4.765	0.994	- [d]	
Synthetic urine [c]	3.0	33.3	12.3	100 (60)	7.050	0.991	- [d]	
	7.0	16.7	8.2	97 (60)	5.426	0.994	16	0.026
		33.3	12.3	100 (60)	7.124	0.993	23	0.055
		66.7	15.7	100 (50)	9.783	0.994	33	0.098
	9.0	33.3	12.4	83 (60)	2.923	0.996	- [d]	
Pt anode								
0.050 M Na_2SO_4 [a]	3.0	33.3	6.4	56 (120)	0.654	0.989	9.4	2.09
	7.0		7.4	49 (120)	0.568	0.988	5.4	4.22
	9.0		7.6	47 (120)	0.535	0.995	4.3	5.44
Urban wastewater [b]	3.0	33.3	6.9	98 (60)	5.687	0.988	- [d]	
	7.0		7.1	93 (60)	4.434	0.994	16	0.922
	9.0		6.7	90 (60)	3.710	0.984	- [d]	
Synthetic urine [c]	3.0	33.3	6.7	100 (60)	5.597	0.990	- [d]	
	7.0		7.7	93 (60)	4.687	0.996	18	0.044
	9.0		7.8	66 (60)	1.815	0,985	- [d]	
IrO_2 anode								
0.050 M Na_2SO_4 [a]	3.0	33.3	6.1	45 (120)	0.427	0.983	6.2	3.03
	7.0		6.6	41 (120)	0.440	0.993	3.5	5.80
	9.0		6.7	38 (120)	0.417	0.991	2.2	9.37
Urban wastewater [b]	3.0	33.3	6.4	91 (60)	3.290	0.981	- [d]	
	7.0		6.5	83 (60)	3.019	0.987	13	1.04
	9.0		6.2	80 (60)	2.830	0.987	- [d]	
Synthetic urine [c]	3.0	33.3	6.3	87 (60)	3.429	0.991	- [d]	
	7.0		6.1	66 (60)	1.811	0.998	12	0.052

9.0	6.1	43 (60)	0.941	0.989	- [d]

Electrolysis time and initial TOC: [a] 120 min and 25 mg L^{-1}, [b] 60 min and 37 mg L^{-1}, [c] 60 min and 745 mg L^{-1}

[d] Not determined

Table 2.

Percentage of degradation, pseudo-first-order rate constant for captopril decay and its *R*-squared, and percentage of TOC removal and specific energy consumption per unit TOC mass for the treatment at 300 min of electrolysis for the treatment of 2.5 L of drug solutions in different aqueous matrices at pH 3.0 and 35 ºC using a solar pre-pilot flow plant with a Pt/air-diffusion cell connected to a planar photoreactor at liquid flow rate of 180 L h^{-1}.

Medium	[Captopril] (mM)	j (mA cm^{-2})	E_{cell} (V)	% Degradation (time (min))	k_1 (min^{-1})	R^2	% TOC removal	EC_{TOC} (kWh (g TOC)$^{-1}$)
AO-H_2O_2								
0.050 M Na_2SO_4 [a]	0.230	50	11.3	36 (30)	0.015	0.993	3.1	30.1
EF with 0.50 mM Fe^{2+}								
0.050 M Na_2SO_4	0.230	50	10.9	100 (20)	0.326	0.993	17	5.11
SPEF with 0.50 mM Fe^{2+}								
0.050 M Na_2SO_4	0.100	50	11.3	100 (5)	1.128	0.992	33	6.14
	0.230	10	4.2	100 (60)	0.083	0.994	16	0.425
	0.230	30	7.3	100 (40)	0.135	0.995	20	1.75
	0.230	50	10.5	100 (15)	0.452	0.995	25	3.36
	0.460	50	10.8	100 (30)	0.186	0.995	19	2.27
Urban wastewater [b]	0.230	50	24.7	100 (15)	0.551	0.990	28	7.06
Urine 1 [c]	0.230	50	10.3	100 (15)	0.361	0.991	70	0.144
Urine 2 [d]	0.230	50	10.1	100 (20)	0.265	0.994	44	0.116
Urine 3 [e]	0.230	50	10.7	98 (30)	0.185	0.992	26	0.112

Initial TOC: [a] 25 mg L^{-1}, [b] 37 mg L^{-1}, [c] 205 mg L^{-1}, [d] 385 mg L^{-1}, [e] 745 mg L^{-1}